On the Application of Cavity Ringdown Spectroscopy to Measurements of Line Shapes and Continuum Absorption

John G. Cormier[*], Joseph T. Hodges[*], and James R. Drummond[#]

[*] *Chemical Science and Technology Laboratory, National Institute of Standards and Technology, 100 Bureau Drive, Gaithersburg, MD 20899, USA*
[#] *Department of Physics, University of Toronto, 60 St. George Street, Toronto ON, M5S 1A7, Canada*

Abstract. Cavity ringdown spectroscopy (CRDS) is a highly sensitive spectroscopic technique that has been successfully applied to problems such as trace gas detection and the observation of weak spectra. Despite possessing several intrinsic advantages over other techniques, CRDS has not yet been widely used to study spectral line shapes. Therefore, we begin with an introduction to CRDS, followed by a discussion of practical considerations and quantitative data analysis for an important variation of CRDS: high-resolution CRDS. We then briefly discuss the features and objectives of two high-resolution CRDS experiments in our laboratory. The first experiment uses a continuous wave CO_2 laser operating in the 920 cm^{-1} to 1090 cm^{-1} region. The principal objective of this experiment is to make accurate measurements of water vapor continuum absorption. The second experiment uses an external cavity diode laser operating in the 10500 cm^{-1} to 10860 cm^{-1} region. This experiment utilizes the frequency comb of a length-stabilized ringdown cavity to provide a precise measure of frequency intervals in line shape measurements. High resolution spectra of a pressure-broadened water vapor transition are presented.

INTRODUCTION

Cavity ringdown spectroscopy (CRDS) is a relatively new technique in which the absorption coefficient of a gas sample is accurately obtained from measurements of the loss rate of optical energy stored inside a high-finesse, stable optical resonator known as the "ringdown cavity" [1-11]. In the past decade, there has been an explosion of growth in the number of CRDS-related journal articles. Our survey of these articles suggests that interest in CRDS is roughly evenly split between the following two applications: 1. Measurement of absorber amount (including trace gas detection), and 2. Observation of weak absorption spectra.

Despite possessing numerous advantages, there are few accounts of CRDS being used to measure spectral line shapes or continuum absorption [8, 10-12]. One of the most important (and oft-discussed) advantages of CRDS is the high sensitivity to weak

CP645, *Spectral Line Shapes: Volume 12, 16th ICSLS*, edited by C. A. Back
2002 American Institute of Physics 0-7354-0100-4

absorption that is possible in the small volume of a typical ringdown cavity. For example, in a CRDS experiment operating near 760 nm, a noise-equivalent absorption coefficient of 5×10^{-10} cm^{-1} $Hz^{-1/2}$ was measured using a 30 ml volume ringdown cavity [8]. Other important advantages include the inherent accuracy of direct absorption measurements, a relatively simple experimental design, a large dynamic range, and impressive signal-to-noise ratio.

CRDS possesses a further advantage that is especially relevant for line shape studies: the possibility of high spectral resolution ($\leq$ 1 MHz), even with pulsed laser sources. This possibility, realizable in high-resolution CRDS [7, 8, 10, 11], exploits the extremely narrow instrumental line widths inherent to high-finesse optical cavities. High-resolution CRDS was also used to achieve the lowest reported relative uncertainties in decay time constants, 3×10^{-4}, corresponding to a signal-to-noise ratio > 3000:1 [8]. Thus, the main purpose of this paper is to encourage the development of high-resolution CRDS experiments for applications requiring high accuracy, sensitivity and spectral resolution. Line shape phenomena that should be interesting to study with high-resolution CRDS include Dicke narrowing, collision-time asymmetry, speed-dependent effects, line mixing, line shifting and far-wing absorption.

We begin with a discussion of practical considerations and quantitative analysis for high-resolution CRDS experiments. Rather than present a comprehensive treatment of the physics of ringdown cavities, we refer the reader to the more detailed discussions given in Refs [4, 5, 7, 11]. Then, we briefly describe the features and objectives of two high-resolution CRDS experiments in our laboratory. One experiment, dubbed MIR-CRDS, uses a continuous-wave (cw) CO_2 laser and operates in the mid-infrared region of 920 cm^{-1} to 1090 cm^{-1}. The other experiment, dubbed NIR-CRDS, uses a cw external cavity diode laser and operates in the near-infrared region of 10500 cm^{-1} to 10860 cm^{-1}.

PRACTICALITIES OF HIGH-RESOLUTION CRDS

In CRDS, laser energy is injected into the ringdown cavity via the transmission of the front mirror (Fig. 1). Following the abrupt termination of the laser excitation, the time evolution of the energy stored inside the ringdown cavity is measured with a fast detector through the transmission loss of the back mirror. The ringdown cavity is usually designed no differently from a spherical mirror Fabry-Pérot interferometer (useful reviews of Fabry-Pérot theory and design may be found in many books and articles, *e.g.* [13]). In general, the ringdown cavity length will have to be precisely controlled, and so a piezoelectric transducer (PZT) is usually incorporated into the design in order to translate one of the mirrors. The best mirrors for CRDS are high-reflectivity dielectric coatings on transparent super-polished substrates having negligible bulk absorption. Dielectric mirror reflectivities vary substantially depending on the spectral region. Mirror reflectivities as high as R = 0.99999 have been employed in a CRDS experiment near 12900 cm^{-1} [14]. However, CRDS has also been

successfully implemented with mirror reflectivities as low as R = 0.994 in the 1000 cm^{-1} region [10].

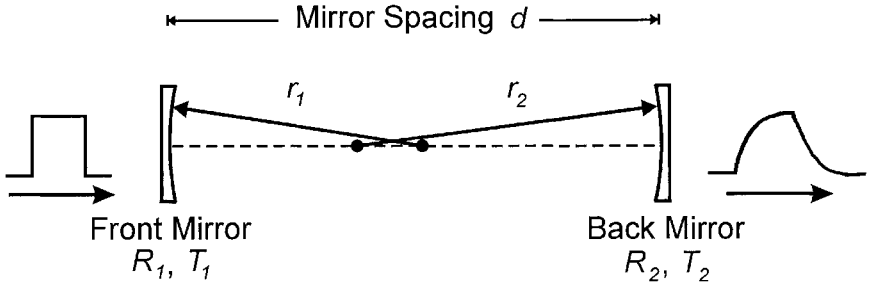

FIGURE 1. Conceptual schematic of a CRDS experiment. The ringdown cavity is formed by two concave, high-reflectivity mirrors spaced a distance *d*. The time evolution of the optical energy stored in the ringdown cavity is sensed with a fast detector via the transmission loss of the back mirror.

It is well known that self-reproducing stable electromagnetic field patterns, or "optical modes", exist inside optical cavities. The cavity eigenmodes are transverse electromagnetic (TEM) modes, which are well approximated by the product of Hermite and Gaussian functions when Cartesian coordinates are used [15, 16]. These modes are designated TEM_{mnq} where *m* and *n* are positive integers identifying the transverse mode orders in the *x*- and *y*-directions, respectively, and *q* is the longitudinal mode order. The lowest order transverse mode of a cavity is the axisymmetric TEM_{00q} mode, corresponding to a Gaussian spatial profile. The eigenfrequencies ν_{mnq} (Hz) for the case of a symmetric cavity are:

$$\nu_{mnq} = \frac{c}{2n_0 d}\left[q + \frac{2}{\pi}(m + n + 1)\arctan\sqrt{\frac{d}{2r-d}} + \frac{\theta}{\pi}\right] \qquad (1)$$

where n_0 is the real part of the refractive index of the cavity medium, *r* is the mirror radius of curvature, and *d* is the cavity length. The term θ represents the phase shift per reflection from the mirrors. The quantity $c/(2n_0 d)$ is an important parameter known as the free spectral range (FSR) of the cavity. The full width at half-maximum (FWHM) of the cavity transmission peaks is given by [17]:

$$\Delta\nu_{FWHM} = \frac{\Delta\nu_{FSR}}{finesse} = \frac{c\sum L_i}{2\pi n_0 d\sqrt{1-\sum L_i}} \qquad (2)$$

where ΣL_i is the sum of all per-pass losses in the cavity, including mirror losses, absorption of radiation by the gas, *etc.* For example, a 1-m long ringdown cavity with $\Sigma L_i = 10^{-3}$ will have $\Delta\nu_{FSR}$ = 150 MHz and transmission peak widths $\Delta\nu_{FWHM}$ = 50 kHz. Thus, the instrument functions of ringdown cavities are comb-like patterns of narrow transverse modes that are repeated over frequency intervals equal to one cavity FSR.

In conventional CRDS, several transverse and/or longitudinal cavity modes may be excited depending on the spatial and spectral overlap of excitation laser energy with cavity modal energies. However, this is unsuitable for high-resolution applications such as line shape measurements, because a multi-peaked instrument function will smear the recorded line shapes. The analysis of multi-mode CRDS signals is also problematic because we have found different optical modes possess significantly different decay rates that do not vary in a predictable way. The modal variation of decay time constants is thought to occur because the mirror surfaces sampled by the different transverse modes have different effective reflectivities, but this hypothesis is difficult to verify. Finally, multi-mode CRDS signals are often distorted by effects such as mode-beating between optical modes, which introduce additional uncertainty to the decay rate measurement [5].

High-resolution CRDS avoids these complications by probing only the TEM_{00q} mode of the ringdown cavity, through a combination of mode-matching and careful selection of cavity geometry (*i.e.* mirror curvature r and separation d). First, the cavity geometry is chosen in such a way that spacing between the lowest-order transverse modes of the cavity is much greater than the bandwidth of the probe laser. This will also prevent the excitation of multiple longitudinal cavity modes. For example, if the laser bandwidth is 60 MHz, then it is necessary to space the TEM_{01q} mode at least 60 MHz away from the TEM_{00q} mode. This could be achieved with a ringdown cavity of length d = 50 cm and r = 80 cm mirrors, as the mode separation would be 110 MHz. In fact, countless combinations of r and d would be suitable. However, exactly confocal cavities ($r = d$) should be avoided, because optical mode degeneracy greatly complicates the task of establishing single-mode excitation.

The laser beam is then mode-matched to the ringdown cavity. Mode matching is a standard technique employing lenses to modify the spot size and phase-front curvature of a propagating Gaussian beam to exactly overlap the TEM_{00q} mode volume of an optical cavity [18, 19]. An ideal Gaussian laser beam may be mode-matched to the TEM_{00q} mode of the ringdown cavity using a single mode-matching lens. However, mode-matching a real laser beam often requires a combination of lenses and/or spatial filter. Fortunately, it is not necessary to achieve perfect mode-matching in high-resolution CRDS. Rather, the goal is to reduce as much as possible the coupling of laser energy into higher order cavity modes, thereby ensuring that the TEM_{00q} mode can be unambiguously identified in the comb-like cavity spectrum. From the spectra of excited cavity modes in our experiments, we typically find that the TEM_{00q} mode has a relative coupling efficiency of $\geq$90%, the TEM_{01q} mode has a relative coupling efficiency of $\leq$10%, and higher order modes have negligible relative coupling efficiencies. The TEM_{00q} mode is therefore always easy to identify in cavity spectra.

The general principle we have developed to achieve high-resolution in our CRDS experiments involves locking the narrow TEM_{00q} mode of a high-finesse ringdown cavity to the output of a cw gas laser. The high intrinsic frequency stability and narrow bandwidth of cw gas lasers provide sufficient precision for high-resolution work. In one of the experiments described below, the MIR-CRDS experiment, the cw gas laser is a stable CO_2 laser (measured drift rate: $\leq$ 5 MHz/day) that also serves as the

ringdown excitation laser. Although the MIR-CRDS experiment does not presently have the fine-tuning range needed to study near-center line shapes, the CO_2 laser is line-tunable over a broad range and so the experiment is very useful for measuring absorption spectra that vary slowly with frequency, such as the infrared water vapor continuum [10, 11]. Of course, gas lasers are unsuitable source lasers for most line shape investigations, and this problem is addressed in the second experiment described in this paper, the NIR-CRDS experiment. Here the ringdown cavity is actively length-stabilized to a cw frequency-stabilized HeNe laser (measured drift rate: $\leq$ 1 MHz/day) and a single-mode external cavity diode laser is used for ringdown excitation and probing of the absorption line shape. In a novel approach, this system uses the stabilized frequency comb of the ringdown cavity as a set of frequency markers for determining frequency intervals of single-mode CRDS spectra. The NIR-CRDS experiment has a fine-tuning scan range large enough to permit near-center line shape investigations. More details on both these experiments are provided following our discussion of data analysis.

QUANTITATIVE HIGH-RESOLUTION CRDS

In a high-resolution CRDS experiment with an unsaturated absorber obeying the Beer-Lambert law, one observes a simple exponential decay of intra-cavity intensity I:

$$I(\nu_{mnq},t) = I_0(\nu_{mnq})\exp(-t/\tau(\nu_{mnq})) + I_b(\nu_{mnq}) \tag{3}$$

where I_0 is the signal at time $t = 0$, I_b is the zero-signal background and τ is the decay time constant. Hereafter the mode index, mnq, associated with the cavity eigenfrequency is omitted for greater clarity. The decay time constant is inversely proportional to the sum of the losses per unit length within the cavity, and is given by:

$$\frac{1}{c\tau(\nu)} = \frac{1}{d}\sum L_i = \frac{1-R(\nu)}{d} + k_{bg}(\nu) + k(\nu) \tag{4}$$

where $R(\nu)$ is the effective reflectivity of the mirror pair and $k_{bg}(\nu)$ encompasses all losses due to the presence of a buffer gas. Here $k(\nu) = N\sigma(\nu)$ is the absorption coefficient of the absorbing gas, where N is the absorber number density and $\sigma(\nu)$ is the absorption cross section.

When the absorber gas is removed from the ringdown cell, Eq. (4) reduces to:

$$\frac{1}{c\tau_0(\nu)} = \frac{1-R(\nu)}{d} + k_{bg}(\nu) \tag{5}$$

where τ_0 is the absorptionless decay time constant. Then, Eq. (4) and Eq. (5) may be rearranged to solve for the absorption coefficient:

$$k(\nu) = \frac{\tau_0(\nu) - \tau(\nu)}{c\tau_0(\nu)\tau(\nu)} \tag{6}$$

Thus, the absorption coefficient is directly obtained from measurements of the decay time constant alone, and in particular does not require separate measurements of both the ringdown cavity length and the mirror reflectivity.

We conclude this section by sharing some of our experience on CRDS data analysis. We have generally found that the best results are obtained when individual decay events are analyzed separately. We do not recommend the common practice of averaging (or "stacking") decay events before solving for the decay time constant. Signal averaging leads to an underreporting of decay time constant uncertainty, and may also mask important diagnostic clues in individual decay events pointing to problems such as multi-mode excitation and nonlinear detection system response. Such clues may include structured residuals due to mode beating, and correlation of decay time constant with peak signal intensity. We also do not recommend taking the logarithm of the background-corrected data (in order to do a linear fit) where the zero-signal background is estimated from pre- (or post-) trigger quiescent signals. This extrapolation of background intensity may significantly bias the fitted decay time constant [11]. Instead, we recommend using the Levenberg-Marquardt least-squares minimization algorithm to fit a fixed portion of each decay curve to Eq. (3). Thus, three free fit parameters are associated with each decay event: the initial intensity, I_0, the decay time constant, τ, and the constant zero-signal background I_b.

MIR-CRDS EXPERIMENT

The layout for the mid-infrared MIR-CRDS experiment is illustrated in Fig. 2. The laser source is a stable cw CO_2 laser that is line-tunable from 920 cm^{-1} to 1090 cm^{-1}.

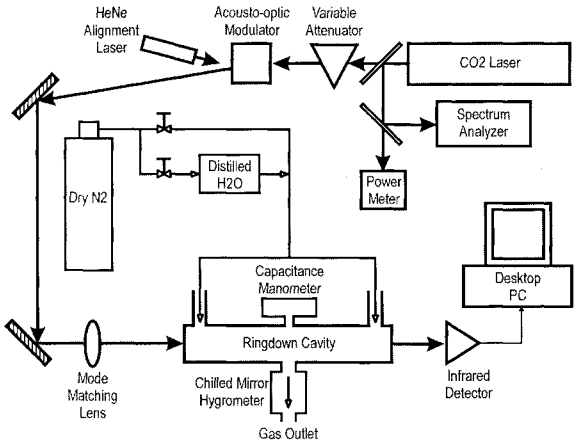

FIGURE 2. Schematic layout for the MIR-CRDS experiment. The main optical beam moves anticlockwise through the apparatus from the CO_2 laser at top right, to the detector at bottom right [10].

At $\tilde{\nu} = 944.195$ cm^{-1}, the 10P(20) transition of CO_2, the laser has a bandwidth

< 120 kHz (1-second measurement) and an output power of 6 W. The laser beam is attenuated with stacked Brewster plates so that only 1 mW of power is incident on the ringdown cavity. Optical pulses (5 μs long) are shaped from the first-order deflected beam of an acousto-optic modulator (AOM) at a repetition rate of 2.5 kHz. The pulses are mode-matched to the ringdown cavity using a single lens (focal length = 75 cm).

The ringdown cavity is formed from two $r = 100$ cm mirrors that are kinematically mounted onto a spacer assembly ($d = 102.5$ cm) designed around three zero-expansion ceramic glass rods (linear expansion coefficient $\alpha = 0.00 \pm 0.02 \times 10^{-6}$ °C^{-1} over the temperature range 0 °C to 50 °C). The 2.54 cm diameter mirrors are made from dielectric coatings layered on ZnSe substrates, and have reflectivity $R = 0.994$ over the spectral range of the CO_2 laser. Horizontal and vertical tilt adjustments of the mirror mounts are made with precision alignment screws. A PZT mounted at one end of the ringdown assembly permits the apparatus to be fine-tuned over 170 MHz, which is slightly greater than the cavity FSR of 146 MHz.

The entire ringdown cavity assembly rests on a three-point kinematic mount inside an electropolished stainless steel gas cell. Infrared radiation enters and exits the gas cell via anti-reflection coated ZnSe windows on the end flanges. Infrared energy exiting the gas cell is sensed with a liquid-nitrogen cooled HgCdTe photovoltaic detector (50 MHz electrical bandwidth). The signal from the dc-coupled output of the detector is digitized by a 12-bit flash converter at a sampling rate of 10^7 s^{-1} and stored on a lab computer for later analysis.

The main objective of the MIR-CRDS experiment is to make accurate measurements of an absorption phenomenon known as the water vapor continuum. The water vapor continuum spans the infrared spectrum and plays a significant role in atmospheric radiative transfer. Despite its importance, we have found large uncertainties in water vapor continuum absorption coefficients, which we discuss separately in an upcoming article [20]. Such uncertainties are certainly forgivable, given the formidable experimental and theoretical challenges that the water vapor continuum has posed since its existence was predicted in 1938 [21]. However, present-day concerns about the possibility of global climate change are adding a sense of urgency to our effort to accurately characterize water vapor continuum absorption so that we may better understand the role it plays in atmospheric radiative transfer.

The chief experimental difficulty arises from the combination of small continuum absorption cross sections and the low saturation vapor pressure of water vapor, resulting in absorption that is too weak for reliable detection in the generally restricted path lengths of the laboratory. In order to measure continuum absorption, investigators have employed a variety of signal-enhancing techniques, most notably large multi-pass cells (*i.e.* White cells) and photoacoustic spectroscopy. However, with uncertainties in water vapor continuum absorption coefficients ranging from ± 20 % for the self-broadened continuum to ± 70 % for the foreign-broadened continuum [11, 20], improved experimental techniques are clearly necessary.

Because it is not possible to detune the experiment from the absorption feature in the case of continuum absorption, we have developed a novel gas flow methodology. Nitrogen gas continuously flows through the ringdown cavity and is exhausted into the

laboratory. By diverting a portion of the inlet gas stream over a body of distilled water prior to entering the ringdown cavity, we are able to generate humidities in the ringdown cavity ranging from zero to near-saturation. The gas flow methodology permits the most non-perturbative continuum measurement possible, in that the only change to the ringdown cell is the amount of water vapor in the gas flow. Another benefit of this approach is that it is possible to make water vapor absorption measurements for several different cell humidities in a short amount of time.

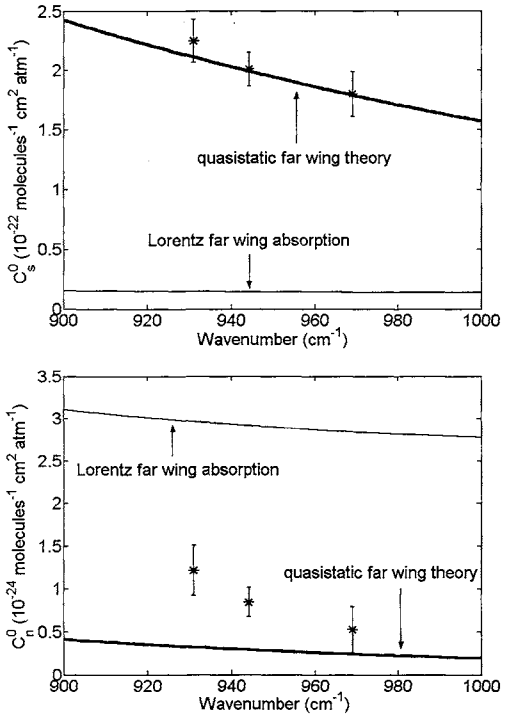

FIGURE 3. Water vapor continuum absorption coefficients in the 900 cm^{-1} to 1000 cm^{-1} region. The self-broadened coefficients are in the top panel and the nitrogen-broadened coefficients are in the bottom panel. Our data are shown as '*' with standard uncertainty error bars. Theoretical calculations of far wing absorption based on the quasistatic approximation are shown as a thick curve [22-24]. For comparison, we also show the far wing absorption calculated using the familiar Lorentz line shape (thin curve).

The MIR-CRDS measurements of continuum absorption coefficients in the 900 cm^{-1} to 1000 cm^{-1} region for $T = 296$ K are presented in Fig. 3. Presently, our experimental results have uncertainties of ± 7 % and ± 20 % in the self- and nitrogen-broadened continuum coefficients, respectively. The generally good agreement between our results and theoretical calculations of far wing absorption provides compelling evidence that the water vapor continuum results from the accumulated far wings of strong water vapor absorption lines [22-24]. This is important, as it has been widely misunderstood that the water vapor continuum results from water vapor dimers since this mechanism was first proposed in 1967 [25, 26]. Our measurements of the water vapor continuum are also significant in that they illustrate the degree to which high-resolution CRDS is free of the baseline drift problems that plague most other experimental techniques.

Ongoing work with the MIR-CRDS experiment is aimed at extending the capability of the apparatus to include studies of temperature dependence. Few low-temperature measurements of the water vapor continuum have ever been attempted due to the extreme sensitivity required; yet accurate continuum coefficients for temperatures ranging from 250 K to 300 K are

necessary for atmospheric radiative transfer applications. In addition, we are also preparing to study the foreign-broadened continuum in greater detail, by measuring the effect of other atmospheric gases such as oxygen and argon. Finally, we also plan to extend the spectral coverage of our data.

NIR-CRDS EXPERIMENT

The layout for the external cavity diode laser NIR-CRDS experiment is illustrated in Fig. 4. The system comprises a symmetric ringdown cavity (r = 100 cm, nominal d = 75 cm) whose length is locked to a frequency stabilized HeNe laser at λ = 633 nm (frequency drift < 1 MHz day^{-1}). A cw external cavity diode laser (ECDL) emitting in the spectral range 920 nm to 940 nm is used as probe laser. The ECDL gives a single-

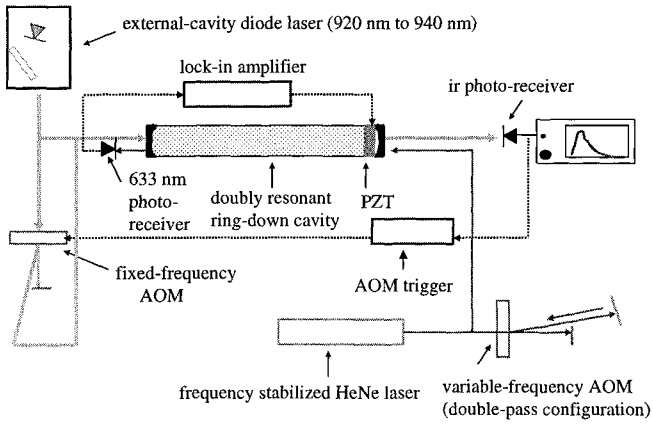

FIGURE 4. Schematic layout for the NIR-CRDS experiment. Numerous optical components have been omitted for clarity. Dashed lines represent electronic connections and solid lines represent visible and infrared laser beams.

mode output (1 s time-averaged linewidth of ≈ 1 MHz) with a mode-hop-free tuning range of 30 GHz. The ringdown mirrors have nominal reflectivities of 0.95 at 633 nm, and 0.99998 near the probe wavelength. A variable frequency AOM is used in a double-pass configuration, thus providing both a variable frequency shift (range of 250 MHz) and frequency modulation (up to 10 MHz) of the 633-nm light without inducing any change in the HeNe beam propagation vector. The instantaneous cavity length is interrogated by measuring the intensity of transmitted HeNe beam with a photodiode. Phase sensitive detection of this transmitted beam at the modulation frequency provides a discriminant signal, which is fed back to actuate the PZT and maintain resonance between the cavity mode frequency and the HeNe laser. This servoing of the cavity length gives time-averaged variations in the FSR ≲ 1 MHz.

At each frequency step, the probe laser frequency is tuned to excite the TEM_{00q} mode of the ring-down cavity. When this signal exceeds a preset value, the probe laser beam is switched off using a fixed frequency AOM. This initiates the passive decay of light from the cavity and gives rise to a single-mode ringdown signal. The process is repeated by increasing the probe laser frequency through one free spectral range of the ring-down cavity to TEM_{00q+1}. In this manner, the frequency steps are independent of nonlinearity, hysteresis and drift in the frequency tuning of the probe laser.

Note that the cavity free spectral range does not limit the minimum frequency step within a spectral scan. Since there is a one-to-one correspondence between the frequency shift of the AOM and the cavity mode spectrum at 633 nm, and since the cavity servo can track changes in the AOM frequency, then for a unit frequency shift in the AOM, the cavity mode frequency spectrum shifts by the amount λ_{HeNe}/λ_p where λ_{HeNe} and λ_p are the wavelengths of the HeNe and probe beams, respectively. In this manner, frequency steps as small as 1 MHz can be realized with the current setup.

Three room-temperature spectra of an isolated transition of water vapor at $\tilde{\nu}$ = 10689.00 cm^{-1} are given in Fig. 5. N_2 was the buffer gas for all cases. The HITRAN database reports a line strength of 1.41×10^{-23} cm^2 cm^{-1} $molecule^{-1}$ and air-broadening parameter equal to 0.0844 cm^{-1}/atm (HWHM) for this transition [27]. The

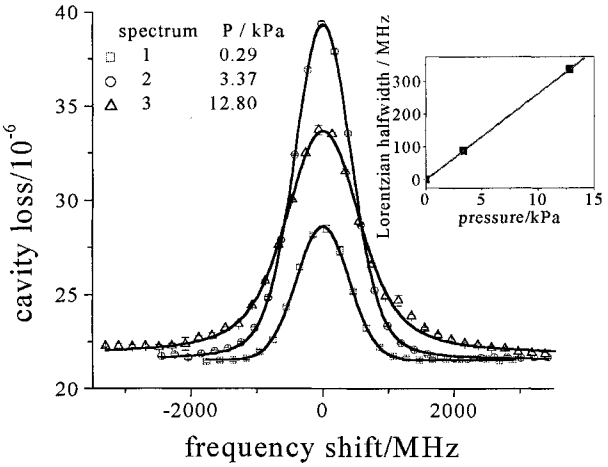

FIGURE 5. Measured single-mode CRDS spectra at 293 K for the 10689.00 cm^{-1} H_2O transition (symbols) and corresponding Voigt fits to the data (solid lines). Spectra 2 and 3 correspond to a fixed partial pressure of H_2O approximately equal to 2.7 Pa (0.02 Torr). The inset shows the Lorentzian halfwidths (squares) derived from the respective fitted data sets and a linear regression to these data (solid line).

first spectrum corresponds to a total pressure of 0.29 kPa (2.2 Torr), and is therefore near the Doppler limit. The expected linewidth based on a Voigt profile and the broadening parameter given above yield a FWHM of 934.4 MHz. The measured

FWHM, based on a fit to the data, gives 937.7 MHz and is within 0.4 % of the predicted value. Spectra 2 and 3 correspond to measurements at a fixed partial pressure of H_2O and total pressure of 3.37 kPa (25.3 Torr) and 12.8 kPa (96.2 Torr) respectively. Voigt fits to the data give best-fit peak areas agreeing to within 0.2 %. Finally, the Lorentzian half width at each pressure was determined from the respective Voigt fits. The results (squares) and a linear least-squares fit of the pressure-dependent data (solid line), are shown in the inset of Fig. 5 and yield an air-broadening parameter 5.2 % greater than the above-reported HITRAN value. While our early results are not yet definitive, they are presented here in order to illustrate the tremendous potential of high-resolution CRDS.

CONCLUSIONS

The main purpose of this paper is to discuss the recent development of high-resolution CRDS experiments and to encourage the application of this powerful technique to line shape investigations. High-resolution CRDS is distinguished from conventional CRDS by the requirements of a length-stabilized ringdown cavity and single-mode excitation. Although instrumental line widths as low as 1 kHz are readily achievable in high-finesse ringdown cavities, this property has rarely been exploited in order to achieve high resolution. One reason is that most CRDS measurements have been performed using non-length-stabilized ringdown cavities, and consequently over the time interval of a spectral scan the frequency comb of the resonator moves about in frequency space. Another reason is that single-mode excitation has not been achieved in most CRDS experiments, which has the effect of limiting the frequency resolution.

In both experiments described herein, length stabilization was achieved by locking the ringdown cavity to the output of a cw gas laser. The first experiment, dubbed MIR-CRDS, uses a cw CO_2 laser as the ringdown excitation laser, and operates in the 920 cm^{-1} to 1090 cm^{-1} region. In this case, the ringdown cavity is passively locked to the CO_2 laser, which is possible due to the impressive stability of both the ringdown cavity and the laser. The primary objective of this experiment is a full and accurate characterization of water vapor continuum absorption. The second experiment, dubbed NIR-CRDS, uses an external cavity diode laser, and operates in the 10500 cm^{-1} to 10860 cm^{-1} region. This experiment actively locks the ringdown cavity to the output of a frequency-stabilized HeNe laser, permitting the frequency comb of the ringdown cavity to be used as precise frequency markers. The NIR-CRDS experiment has a fine-tuning range of 30 GHz, large enough to permit near-center line shape measurements. For both experiments, we have presented early results, and we hope to report on further progress at a later date.

Finally, we note that high-resolution CRDS offers a further tantalizing possibility: high accuracy (*i.e.* sub-MHz uncertainties) determination of the frequency axis in absorption spectra. Although we do not presently make a high-precision measurement of the cavity FSR, one could adopt the method of Bay *et al.* to measure the cavity FSR [28]. Our preliminary analysis suggests that this technique could permit

determination of the cavity FSR to within 10 kHz. It is also interesting to note that this method, which involves frequency modulation techniques, does not require a measurement of the cavity length in order to obtain the FSR of the ring-down cavity. Furthermore, the absolute measurement of laser frequency using a stabilized high-finesse interferometer has already been demonstrated [29], and we believe a similar methodology could be implemented in high-resolution CRDS. In conclusion, high-resolution CRDS experiments based on the general methodologies discussed here could be developed that permit the acquisition of ultra-low uncertainty spectroscopic data. These data could be applied to problems such as atmospheric radiative transfer, atmospheric remote sounding, and the testing of *ab initio* line shape theories.

REFERENCES

1. O'Keefe, A., and Deacon, D. A. G., *Rev. Sci. Instrum.* **59**, 2544-2551 (1988).
2. Romanini, D., and Lehmann, K. K., *J. Chem. Phys.* **99**, 6287-6301 (1993).
3. Zalicki, P., and Zare, R. N., *J. Chem. Phys.* **102**, 2708-2717 (1995).
4. Lehmann, K. K., and Romanini, D., *J. Chem. Phys.* **105**, 10263-10277 (1996).
5. Hodges, J. T., Looney, J. P., and van Zee, R. D., *J. Chem. Phys.* **105**, 10278-10288 (1996).
6. Hodges, J. T., Looney, J. P., and van Zee, R. D., *Appl. Opt.* **35**, 4112-4116 (1996).
7. Looney, J. P., Hodges, J. T., and van Zee, R. D., "Quantitative Absorption Measurements Using Cavity-Ringdown Spectroscopy With Pulsed Lasers," in *Cavity-Ringdown Spectroscopy: An Ultratrace-Absorption Measurement Technique*, edited by K. W. Busch and M. A. Busch, American Chemical Society, New York, 1999, pp. 93-105.
8. van Zee, R. D., Hodges, J. T., and Looney, J. P., *Appl. Opt.* **38**, 3951-3960 (1999).
9. Berden, G., Peeters, R., and Meijer, G., *Int. Rev. Phys. Chem.* **19**, 565-607 (2000).
10. Cormier, J. G., Ciurylo, R., and Drummond, J. R., *J. Chem. Phys.* **116** 1030-1034 (2002).
11. Cormier, J. G., *Development of an Infrared Cavity Ringdown Spectroscopy Experiment and Measurements of Water Vapor Continuum Absorption*, PhD thesis, University of Toronto, 2002.
12. Romanini, D., and Lehmann, K. K., *J. Chem. Phys.* **105**, 81-88 (1996).
13. Vaughan, J. M., *The Fabry-Perot Interferometer: History, Theory, Practice and Applications*, Adam Hilger, Philadelphia, 1989.
14. Romanini, D., Kachanov, A. A., and Stoeckel, F., *Chem. Phys. Lett.* **270**, 538-545 (1997).
15. Boyd, G. D., and Gordon, J. P., *Bell Sys. Tech. J.* **40**, 489-508 (1961).
16. Yariv, A., *Quantum Electronics*, Wiley, New York, 1989.
17. Born, M., and Wolf, E., *Principles of Optics*, 6th ed., Cambridge University Press, New York, 1980.
18. Kogelnik, H., *Bell Sys. Tech. J.* **43**, 334-337 (1964).
19. Kogelnik, H., and Li, T., *Appl. Opt.* **5**, 1550-1567 (1966).
20. Cormier, J. G., and Drummond, J. R., to be published in the forthcoming NATO Science Series volume entitled *Weakly Interacting Molecular Pairs: Unconventional Absorbers of Radiation in the Atmosphere*.
21. Elsasser, W. M., *Phys. Rev.* **53**, 768 (1938).
22. Tipping, R. H., and Ma, Q., *Atmos. Res.* **36**, 69-94 (1995).
23. Ma, Q., and Tipping, R. H., *J. Chem. Phys.* **111**, 5909-5921 (1999).
24. Ma, Q., and Tipping, R. H., *J. Chem. Phys.* **112**, 574-584 (2000).
25. Penner, S. S., and Varanasi, P., *J. Quant. Spectrosc. Radiat. Transfer* **7**, 687-690 (1967).
26. Gebbie, H. A., *et al.*, *Nature* **221**, 143-145 (1969).
27. Rothman, L. S., *et al.*, *J. Quant. Spectrosc. Radiat. Transfer* **60**, 665-710 (1998).
28. Bay, Z., Luther, G. G., and White, J. A., *Phys. Rev. Lett.* **29**, 189-192 (1972).
29. Layer, H. P., Deslattes, R. D., and Schweitzer, W. G. Jr., *Appl. Opt.* **15**, 734-743 (1976).